The Collection of Positive Ions and Electrons by a Screened Probe in the Neon Negative Glow*

M.J. Vasile† and R.F. Pottie,

Division of Applied Chemistry,
National Research Council,
Ottawa, Canada.

INTRODUCTION

The collection of ions and electrons by small probes placed within the plasma of a gas discharge has received considerable attention over the past four decades. A major advance in measurement technique was reported by Boyd[1] in 1950 with the introduction of a small screened flat probe. The new technique made it possible to separate the collected currents into the ion and electron components. As a result it became possible to measure their concentrations separately and to extend the range of measured electron velocities to beyond the ionization potential of the discharged gas with no interference from positive ion current. The method was extended by Boyd and co-workers[2] and by Pringle and Farvis[3] to the measurement of ions and electrons in both the positive column and negative glow in various gases. Despite the apparent success of these studies, little or no use has been made of this technique by other workers in the field.

Previous work in this laboratory[4,5] had established the usefulness of a mass spectrometer to obtain relative ion concentrations in the various regions of glow discharges. The work reported here is an extension of these earlier studies and represents an attempt to (a) measure the absolute concentrations of ions and electrons in conjunction with the mass spectrometric studies and (b) to determine the electron energy distributions, particularly in the negative glow to assist in the interpretation of processes that result in the production of ions.

EXPERIMENTAL

. Apparatus

In order to reduce undue disturbance of the discharge, an essential characteristic of a probe is small size. The probe consisted of a fine wire grid that was spot welded to a 5 × 5 mm platinum frame which was mounted on a Pyrex plate. A 1/8" circular hole in the glass plate defined the current reaching the platinum collector (.010" thick) mounted below it. A mica insulator shielded the collector from the discharge. The glass plate was 1 mm thick, and the grid was a stainless steel mesh (0.001" diameter wires) with an optical transparency of 42%. The effective area of the collector was computed to be 3.33×10^{-6} m^2. The probe parts were cemented together with "Gevac" and the platinum leads (.01" diam.) from the electrodes were supported and insulated by means of a ceramic rod with two channels for the leads. The ceramic rod extended through a side-arm of the discharge tube so that it could be rotated or moved radially by means of a magnetic slug. Impedance measurements showed that the resistance between the collector and grid was greater than 10^{13} ohms.

The Pyrex discharge tube was 50 cm long and 5.5 cm in diameter. The electrodes were polished stainless steel discs, 5 cm in diameter and the cathode could be moved magnetically over a distance of 30 cm. The entire discharge tube, including side-arms, could be baked to greater than 350°C. Metal bellows valves were used for all openings into the discharge tube and the normal background pressure of 2×10^{-7} Torr was achieved with a silicone oil diffusion pump.

The gases were of assayed research grade and periodic checks were made for impurities by mass spectrometry. The operating gas was admitted to the discharge tube via a Granville-Phillips variable leak valve, the pressure being measured with a Decker diaphragm gauge. A small flow was maintained through the discharge tube during operations by means of a needle valve to the pumps. The exit pressure was about 10^{-2} Torr. Preliminary discharges of about one hour duration were always carried out before measurements were taken. The tube was then evacuated and a fresh gas sample was admitted for the experiment.

All results reported here were taken with a gas pressure of 0.28 Torr and a discharge current of 0.250 ma.

A schematic diagram of the discharge tube and electrical circuit is given in Fig. 1. The potentials of the grid and collector relative to the grounded anode could be controlled independently so that either one could be positive or negative with respect to the anode. The collector current passing through precision resistors (0.05%) was measured with a 1 megohm impedance nanovoltmeter which was isolated from ground. The minimum detectable current was 10^{-10}A. The potential of the collector was measured with a vacuum tube voltmeter, while a digital voltmeter was used for measurement of the grid potential. Grid and discharge currents were monitored by dc microammeters. Discharge power was provided by a commercial dc power supply.

B. Results

(1) Collection of low energy electrons. Fig. 2(a) is a typical semi-logarithmic plot of the electron current, showing two straight line segments for the thermal and secondary electrons respectively. The space potential was obtained from extrapolation of the saturation current to the rising portion of the curve. The gas was pure neon and the probe was near the position of maximum electron intensity in the negative glow. The electron temperatures of the Maxwellian distributions were 0.271 and 3.67 eV for the thermal and secondary electrons, and their concentrations were $158 \times 10^{13}/m^3$ and $2.9 \times 10^{13}/m^3$ respectively, assuming collection of the random current at the space potential[6,7]. The small electron residual current that was always observed at higher retardation potentials was subtracted from the total electron currents. The collector potential was +70 V with respect to the anode.

(2) Collection of positive ions. The collector potential was maintained at -70 V and the grid voltage was varied from -70 V to well above the space potential for the collection of positive ions. The method of calculation of the random positive ion current differed somewhat from previous approaches and is given briefly below. We assume that positive ions are accelerated from the sheath to the grid and are further accelerated by the full potential between the collector and the grid. The current rises until all the random ion current arriving at the sheath edge has been collected. Further collection of ion current is the result of sheath expansion, edge effects and potential penetration of the sheath. If we treat the ion currents

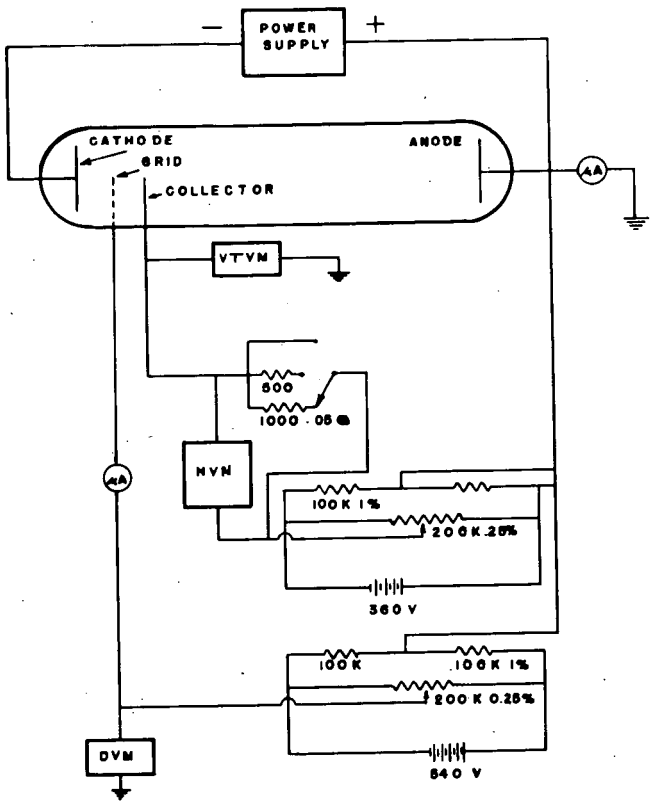

FIG. 1 Apparatus and schematic circuit diagram.

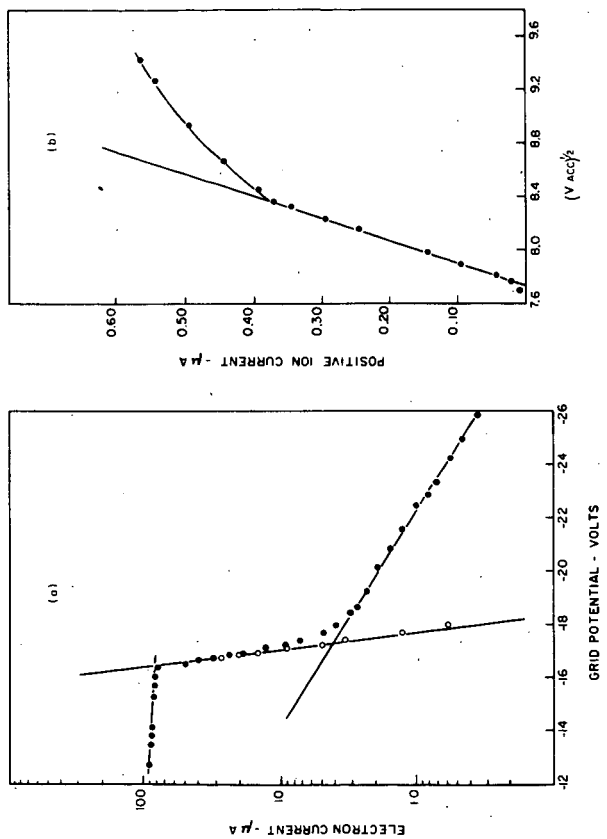

FIG. 2 Collection of ions and electrons in pure neon, distance from grid to cathode = 2.55 cm, probe facing anode. Fig. 2(a) - electron curve, Fig. 2(b) - ion collection curve.

below the saturation limit we find[59]

$$i_+ = A \times \frac{1}{4} n_p \, q \, V_f \qquad (1)$$

in which n_p is the random ion density, q the electronic charge and V_f the velocity of the ions arriving at the collector. This is given by:

$$V_f = V_o + \left(\frac{2qV_{acc}}{m}\right)^{1/2} \qquad (2)$$

in which V_o is the initial ion velocity and V_{acc} is the potential difference between the plasma and the collector. Thus:

$$i_+ = A \times \frac{1}{4} n_p \, q\left(V_o + \left(\frac{2q}{m}\right)^{1/2} V_{acc}^{1/2}\right) \qquad (3)$$

Therefore, a plot of i_+ versus $V_{acc}^{1/2}$ should yield a straight line whose slope is

$$\frac{A}{4} n_p \, q\left(\frac{2q}{m}\right)^{1/2} .$$

The positive ion currents, plotted in this manner always yielded a straight line to a break point which was assumed to be the saturation limit. A plot of this type is shown in Fig. 2 (b); the small residual ion current has been subtracted from the experimental points. From this slope we calculate $n_p = 145 \times 10^{13}/m^3$ in good agreement with the electron concentration of Fig. 2 (a) for the same probe position.

(3) Axial variation of ions and low energy electrons. The observed ion and electron concentrations as a function of axial distance from the cathode are given in Fig. 3 for the probe facing the anode. There is a slight displacement between the maxima for the two distributions and this may reflect a slight penetration of the field from the cathode dark space. However the results show that a true plasma is present in the negative glow, since to a good approximation $n_e = n_p$. The secondary electron current was relatively insensitive to position of the probe and gave an average concentration of $3 \pm 1 \times 10^{13}/m^3$ with electron temperatures in the range of 3.5 - 4.0 eV. The rising portion of the secondary electron curve marks the anode edge of the negative glow. At this point the electric field begins to accelerate thermal electrons to the secondary electron velocities. For example at d = 7.2 cm, the secondaries account for almost 50% of the total electron current.

(4) Residual electron current. Small residual electron currents were observed for all probe positions and orientations. These are summarized in Fig. 4 for pure neon. These minimum currents were constant for a range of -35 to -50 V in grid potential. For grid voltages in excess of -50 V there was a gradual rise in the current, presumably as a result of grid emission by the bombardment of positive ions. We find in Fig. 4 that the residual current decreases exponentially throughout the negative glow with increasing distance from the cathode for both orientations of the probe surface. Additionally, there is a reduction by almost a factor of 5 for the probe facing the anode versus cathode position. We have also observed no variation in the residual current as a function of radial position from the center to a point only 0.6 cm from the wall. The current increases slowly with axial distance in the Faraday dark space (d > 5 cm) and reaches a plateau in the positive column.

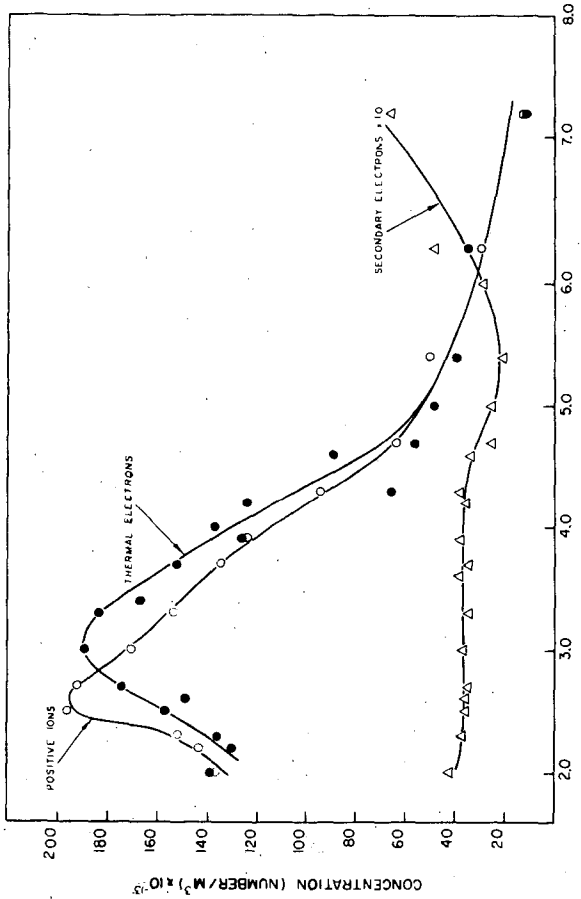

FIG. 3 Distribution of ions and low energy electrons vs. distance between grid and cathode, probe facing anode for pure neon.

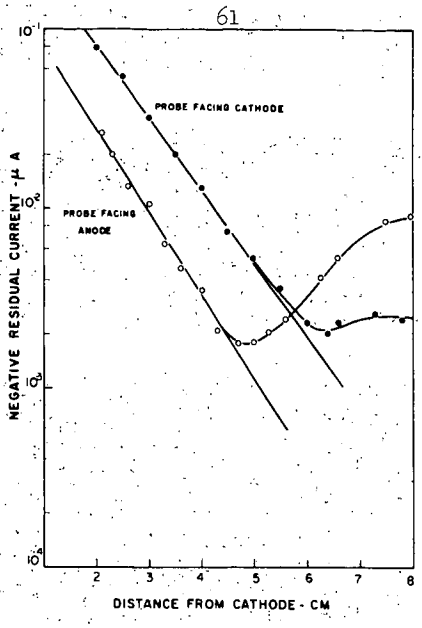

FIG. 4 Variation in residual negative current vs. distance between grid and cathode for pure neon.

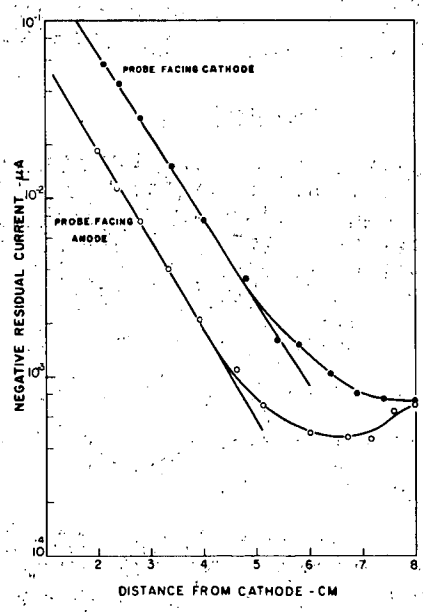

FIG. 5 Variation in residual negative current vs. distance between grid and cathode for 0.07% Xenon in neon.

The effect of adding 0.07% xenon to neon is seen in Fig. 5. The residual current drops and there is a steeper slope to the exponential part of the curve. In addition a smaller increase is observed in the Faraday dark space.

(5) Energy distribution of secondary electrons. From Fig. 2 (a) we see that the energy distribution of secondary electrons is essentially Maxwellian at the indicated position of the probe. However, as the axial distance is increased we find a successively greater loss of electrons whose energies exceed about 10 eV, although the distribution is not radically altered from Maxwellian. The addition of 0.07% xenon results in almost complete depletion of electrons above 12 eV and there are considerable deficiencies beginning only 5 eV above the space potential.

The data are summarized in Fig. 6. The distribution curves for the mixture were calculated from the experimental measurements according to the method of Medicus[8], and comparison plots of the ideal Maxwellian distribution are given. The two curves in each case were normalized to those regions along the potential axis which gave a straight line on the semi-logarithmic plot. The fluctuations in the curves for the mixture were reproducible and are similar in appearance to the structural features that were observed by Twiddy[9] in the cathode region of rare gas discharges. It is apparent that xenon effectively reduces the higher energy secondary electrons, even at 0.07% concentration. Twiddy[10] has shown that there is a similar loss of energetic electrons in the positive column of an argon-neon mixture.

(6) Residual positive ion current. The ratio of residual currents for i_e min/i_+ min was 5:1 with the probe facing the cathode and about 10:1 with the probe facing the anode. These ratios were constant for all axial positions of the probe in the negative glow and in the Faraday dark space. The ratios for the 0.07% xenon-neon mixture were the same as for pure neon.

DISCUSSION

Since the production of ions and low energy electrons in the negative glow is governed largely by the rate of arrival of high energy electrons from the cathode dark space it is obvious that the direct observation of these high energy electrons offers an important method for interpreting the processes of ionization in the negative glow. A possible means of making such a measurement is to consider the negative residual currents collected by the screened probe when it faces the cathode. These currents could arise from several processes:

(a) Direct collection of high energy electrons.
(b) Grid emission by high energy electrons.
(c) Grid emission by bombardment of positive ions.
(d) Grid emission by metastable atom impact.
(e) Grid emission by photon impact.

Rotation of the probe to face the anode caused a 2/3 reduction in the residual current. One would not expect processes (c), (d), and (e) to depend markedly on probe orientation so that these processes probably account for less than 1/3 of the total residual negative current when the probe faces the cathode. Since neither the positive ion density nor the visible photon intensity decays exponentially, processes (c) and (e) are similarly rejected as a major source of current for the anode orientation. We conclude that the major causes of the negative residual current in the negative glow are processes (a) and (b)

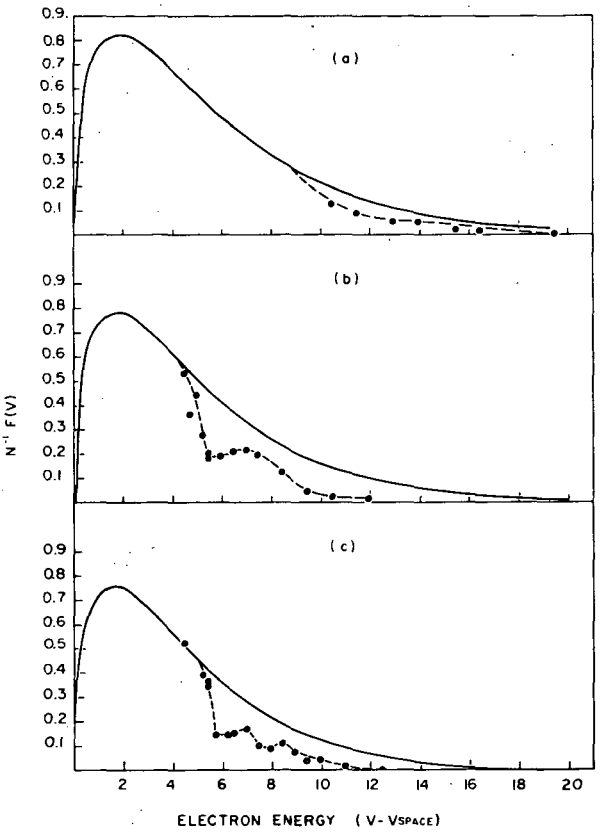

FIG. 6 Energy distribution function of secondary electrons compared with the Maxwellian distribution. (a) pure neon, d = 2.3 cm (b) mixture .07% Xenon in neon, d = 2.2 cm (c) mixture, d = 3.0 cm. Probe facing anode.

for the probe facing the cathode. We cannot distinguish between (a) and (b), nor is it possible to calculate the density of such high energy electrons without knowledge of their velocities.

The observed exponential decrease in i_e min through the negative glow of pure neon (Fig. 4) can be written as:

$$i_d = i_o \exp(-\sigma n(d-d_o)) \qquad (4)$$

in which i_o is the residual current at d_o cm from the cathode, d is the distance of the probe surface from d_o and n is the concentration of neon atoms per unit volume. Thus σ has the dimensions of cm^2 and is an experimental cross section for loss of high energy electrons, as a first approximation. From the slope of the exponential curve in Fig. 4 we calculate that $\sigma = 8.7 \times 10^{-17}$ cm^2. This is a reasonable value since the cross section for ionization of neon[11] by 100 eV electrons is 7.58×10^{-17} cm^2.

The addition of 0.07% xenon brings about a 30% reduction in the negative residual current and the exponential slope increases so that the experimental $\sigma = 1.03 \times 10^{-16}$ cm^2. This cannot be accounted for by assuming that the only additional loss is that arising from the ionization of xenon. At a concentration of only 7×10^{-2} atom %, this would imply a cross section for ionization of xenon equal to 228×10^{-16} cm^2 - about a factor of 40 higher than the known σ_i of xenon[11] for 100 eV electrons. A more reasonable inference is that the loss of neon metastables by the Penning reaction:

$$Ne^*(^3P_{2,0}) + Xe \rightarrow Xe^+ + Ne + e^- \qquad (5)$$

is responsible for the lower values of i_e min, and that the change in slope more nearly reflects the actual stopping power of neon for high energy electrons. Since excitation as well as ionization can result from impact of a high energy electron, a cross section of the order of 1×10^{-16} cm^2 is of the expected magnitude for an electron of approximately 100 eV.

It would be expected that the addition of a small amount of xenon would not significantly change either the cathode fall or the number of directed high energy electrons passing into the negative glow. Thus, if one assumes that the reduction in the residual electron current is caused by reaction (5) it is possible to obtain an approximate value for the concentration of metastables in the beginning of the negative glow.

Referring to Fig. 4, for d = 2 cm, $-\Delta i$, the reduction in the residual current is 0.02 μA. If the neon metastables have thermal velocities, and if one considers a reasonable yield of about 0.03 for the grid emission (geometric factor × efficiency), then a minimum concentration of $1 \times 10^{13}/m^3$ is obtained for the metastables. It is then possible to calculate the reactive collision frequency between Ne* and Xe by assuming the same cross section for deactivation as Sholette and Muschlitz[12] observed for the He* - Xe Penning reaction, namely 12×10^{-16} cm^2. This results in a calculated lifetime for the neon metastables of 0.5 m sec. This is somewhat shorter than the lifetime of 0.875 m sec measured by Blevis et al.[13] for the decay of $Ne(^3P_2)$ in pure neon. We conclude that xenon can intercept the metastable neon atoms in the required time and that our assignment of the Penning reaction is reasonably justified as a major contributing

cause of the reduction in the residual negative current. Similar arguments can be used to account for the decrease in the residual current when the probe faces the anode. The effect is even more marked in this case, particularly at the beginning of the positive column.

The treatment of the positive ion residual current is not as straightforward, since there arises the additional complication of electron impact ionization in the space between the grid and the collector. To a rough approximation we can account for about 60% of the current with the probe facing the cathode by this process, but the remainder can be a combination of secondary emission from the collector by photons, by metastable atoms and by energetic electrons. The very small currents observed for the probe facing the anode suggest that the release of electrons by metastable impact is much less than would be expected for the metastable density obtained above. Apparently the impact of metastables with the platinum surface produces secondary electrons with a much lower efficiency than does the stainless steel grid. The reason is not clear, but a contributing cause may be due to the higher work function of platinum.

REFERENCES

* N.R.C. No. ...., †N.R.C. Postdoctorate Fellow.

1. R.L.F. Boyd, Proc. Roy. Soc. A201, 329 (1950).
2. R.L.F. Boyd and N.D. Twiddy, Nature 173, 633 (1954).
3. D.H. Pringle and W.E.J. Farvis, Proc. Phys. Soc. B68, 836 (1955).
4. P.F. Knewstubb and A.W. Tickner, J. Chem. Phys. 36, 674 (1962).
5. P.F. Knewstubb and A.W. Tickner, J. Chem. Phys. 36, 684 (1962).
6. I. Langmuir and H. Mott-Smith, Jr., G.E. Review 27, 449 (1924).
7. H. Mott-Smith and I. Langmuir, Phys. Rev. 28, 727 (1956).
8. G. Medicus, J. Applied Phys. 27, 1242 (1956).
9. N.D. Twiddy, Proc. Roy. Soc. A262, 379 (1961).
10. N.D. Twiddy, Proc. Roy. Soc. A275, 338 (1963).
11. D. Rapp and P. Englander-Golden, J. Chem. Phys. 43, 1464 (1965).
12. W.P. Sholette and E.E. Muschlitz, Jr., J. Chem. Phys. 36, 3368 (1962).
13. B.C. Blevis, J.M. Anderson, and R.W. McKay, Can. J. Phys. 35, 941 (1957).